

Ising-Bloch Transition in Degenerate Optical Parametric Oscillators

Isabel Pérez-Arjona, Fernando Silva, Germán J. de Valcárcel, Eugenio Roldán,

Departament d'Òptica, Universitat de València,

Dr. Moliner 50, 46100 Burjassot, Spain.

Víctor J. Sánchez-Morcillo

Departament de Física Aplicada, Universitat Politècnica de

València,

Ctra. Nazaret-Oliva S/N, 46730 Grao de Gandia, Spain.

November 21, 2018

Abstract

Domain walls in type I degenerate optical parametric oscillators are numerically investigated. Both steady Ising and moving Bloch walls are found, bifurcating one into another through a nonequilibrium Ising–Bloch transition. Bloch walls are found that connect either homogeneous or roll planforms. Secondary bifurcations affecting Bloch wall movement are characterized that lead to a transition from a steady drift state to a temporal chaotic movement as the system is moved far from the primary, Ising–Bloch bifurcation. Two kinds of routes to chaos are found, both involving tori: a usual Ruelle-Takens and an intermittent scenarios.

1. Introduction

Nonlinear optical systems with broken phase symmetry and high Fresnel number have a tendency to emit light beams whose transverse section displays uniformly illuminated do-

mains (usually spatially homogeneous) separated by dark lines, the so-called domain walls (DWs). These structures are also commonplace in self-oscillatory chemical reactors (like some variants of the BZ reaction) forced at a 2:1 resonance, and in weakly damped nonlinear mechanical systems (chains of coupled pendula, or fluids) when parametrically forced. In both cases, sustained waves appear that oscillate at half the driving frequency. An optical analogue of this is the degenerate optical parametric oscillator (DOPO): a $\chi^{(2)}$ cavity is driven by a coherent light field of frequency 2ω and the system starts to oscillate (above a certain threshold) at the subharmonic frequency ω .

Examples of DWs have been predicted to occur in the last few years in several nonlinear optical resonators, such as DOPOs¹⁻⁵, vectorial Kerr cavities^{6,7}, type II second harmonic generation⁸ and, importantly, have also been experimentally realized in parametric mixing^{9,10}. Related phenomena have also been reported in nascent optical bistability¹¹, in which case domains of low and high light intensity are separated (or better, joined) by a switching front, and in single feedback mirror experiments in the presence of an intrinsic polarization instability¹², where domain patterns are observed.

Usually a DW asymptotically joins two homogeneous states, u_{\pm} . In the simplest, most usual case, u_{\pm} have the same amplitude and opposite phase, i.e. $u_{+} = -u_{-}$, corresponding to two antisymmetric fixed points in the complex plane $\langle \text{Re } u, \text{Im } u \rangle$. In this representation, a trajectory connecting the two domains can follow two paths, corresponding to two different types of walls: either crossing the complex zero (Ising wall) or surrounding it (Bloch wall). In terms of the phase, in an Ising wall there is a discontinuous variation of the field phase across the wall whereas in a Bloch wall the phase angle rotates through π across the wall. This is a crucial difference between Ising and Bloch walls as it implies that the latter are chiral while the former are not. The chirality measures the direction and magnitude of the rotation of the phase angle at the wall core and, as two directions of rotation of the phase angle can in principle be expected, Bloch walls of positive and negative chirality can exist. Alternatively, in an Ising wall the field intensity vanishes at its core, whilst it is minimum, but not zero, in a Bloch wall. That is the reason why in nonlinear optics Ising and Bloch

walls are sometimes referred to as dark and grey solitons, respectively.

In nonequilibrium systems, Ising walls bifurcate into Bloch walls by varying a parameter of the system, the bifurcation point corresponding to the nonequilibrium Ising-Bloch transition¹³ (NIB in the following). In systems showing this behaviour, the chirality behaves as an order parameter, and can be described, in principle, by a nonlinear evolution equation: the NIB transition is then related to a bifurcation of the chirality parameter¹⁴. Importantly, in gradient systems (those whose dynamics derives from a potential), both Ising and Bloch walls are at rest. This is a consequence of the equivalence between the states connected by the wall, characterized by the same free energy. However, in nongradient systems, such as the DOPO, a generic property of Bloch walls is that they move with a velocity proportional to (or related with) their chirality, while Ising walls are at rest¹⁴.

The NIB transition has been found in systems of very different nature, such as nematic liquid crystals¹⁵, and reaction-diffusion systems¹⁶. In the context of nonlinear optics, it has been found in type II optical parametric oscillators when cavity birefringence and/or mirror dichroism are taken into account⁶, and in type II second harmonic generation⁸. It has also been studied in universal equations describing nonlinear optical cavities in some limiting cases, as it is the case of the parametrically driven Ginzburg–Landau equation¹⁷ and the parametrically driven nonlinear Schrödinger (PDNLS) equation¹⁸. In⁸ a universal criterion for evaluating the NIB transition boundary in a wide variety of nongradient systems was proposed.

The results obtained in¹⁸ are particularly relevant for the present work. Whilst it is well known that the PDNLS equation with self–defocusing nonlinearity exhibits domain walls (tanh solitons)²⁰, it was not known until recently¹⁸ that domain walls are also solutions of this equation when the nonlinearity is self–focusing (in which case the basic solitonic structure is a sech). This fact makes possible that the same nonlinear system exhibits both bright and dark solitons in adjacent regions of the parameter space, as bright solitons are stable solutions of the PDNLS equation¹⁹. Moreover, in¹⁸ it was shown that a NIB transition occurs in this equation. It is to be remarked that the DWs found in the self–

focusing PDNLS equation can connect not only homogeneous states, as usual domain walls do, but also patterned states. As that equation has been derived in nonlinear optics for a number of systems (in particular for DOPOs with large pump detuning¹, vectorial Kerr cavities with large cavity anisotropy⁷, and fiber rings with phase-sensitive amplification²¹) the results presented in¹⁸ imply that these systems should exhibit domain walls and a NIB transition in some parameter range.

In this paper we show numerically that the Ising walls previously studied in the type I DOPO can experience the NIB transition for positive signal detuning. Remarkably, we show that this occurs in a parameter domain for which the PDNLS equation, which was derived for large pump detuning¹, cannot be applied. The moving Bloch fronts that appear beyond the NIB bifurcation connect two homogeneous states with opposite phase and exist in a finite parameter region. By varying a control parameter (e.g., the signal detuning) the homogeneous solutions connected by the Bloch wall become modulationally unstable and are replaced by rolls. These new domain walls exhibit a very rich dynamic behaviour that we analyze in detail. We would like to mention that some of the results presented here have been previously found by Le Berre *et al.*⁴ in a propagation model for DOPO. In particular, they pointed out that DWs exist in the DOPO also for positive signal detuning, that these domain walls can connect patterned states, and it was also speculated by the authors that the system could exhibit a NIB transition. The main goals of the present work are to characterize the NIB transition in DOPOs and to describe in detail the nonlinear dynamics of the Bloch walls. Our study, being specific of the DOPO model, finds however a qualitative parallelism with our previous work on the PDNLS equation¹⁸; we thus conjecture that our findings should be applicable to other systems.

2. Model, homogeneous solutions and their stability

The standard, mean-field model for a type I DOPO reads²²

$$\frac{\partial A_0}{\partial T} = \gamma_0 \left[-(1 + i\Delta_0)(A_0 - E) - A_1^2 + ia_0 \nabla^2 A_0 \right], \quad (1)$$

$$\frac{\partial A_1}{\partial T} = \gamma_1 \left[-(1 + i\Delta_1)A_1 + A_0 A_1^* + ia_1 \nabla^2 A_1 \right], \quad (2)$$

where A_n are the slowly varying envelopes of the intracavity pump ($n = 0$) and signal ($n = 1$) fields, γ_n, Δ_n and a_n their corresponding cavity decay rates, detuning and diffraction coefficients, and E is the amplitude of the injected pump, which in general may depend on transverse coordinates. The phase-matching condition imposes that $\gamma_0 a_0 = 2\gamma_1 a_1$. In this paper we shall consider the 1D limit of Eqs. (1). This situation corresponds, e.g., to a slab waveguide configuration for the resonator, in which the fields are confined in one direction of the transverse plane, say Y , the diffraction acting only in the X direction, and then $\nabla^2 = \partial^2/\partial X^2$. In the following we shall concentrate in the particular case $\gamma_0 = \gamma_1 \equiv \gamma$ (hence $a_1 = 2a_0$), and use normalized time $t = \gamma T$ and space $x = X/\sqrt{a_1}$. Moreover, throughout this paper we shall assume that the two fields oscillate within the same cavity and then we shall keep the relation $\Delta_0 = 2\Delta_1$ fixed.

For a spatially uniform injected pump, Eqs.(1) and (2) admit two homogeneous solutions. The trivial solution $\{A_0 = E, A_1 = 0\}$ exists for all parameter sets, while the "lasing" solution

$$\begin{aligned} |A_1|^2 &= \Delta_0 \Delta_1 - 1 \pm \sqrt{E^2(1 + \Delta_0^2) - (\Delta_0 + \Delta_1)^2}, \\ |A_0|^2 &= 1 + \Delta_1^2, \end{aligned} \quad (3)$$

that corresponds to the subharmonic (signal) generation, requires a threshold pump. The bifurcation from the trivial solution to the lasing solution (3) occurs at $E = \sqrt{1 + \Delta_1^2}$; it is subcritical (and then the lasing solution can coexist with the stable trivial state) when $\Delta_0 \Delta_1 > 1$, and is supercritical in the opposite case²³. For positive Δ_1 (which is the case we consider throughout the paper) this is the only bifurcation that affects the trivial state. Note that the discrete phase symmetry $A_1 \rightarrow -A_1$ supported by Eqs.(1) and (2) makes that two equivalent solutions of equal intensity but opposite phase exist and are dynamically equivalent, and this opens the possibility of exciting DWs connecting them. For negative

Δ_1 (a case we do not discuss here) a pattern forming instability affecting the trivial state occurs at $E = 1^{22}$ leading to the appearance of roll patterns²⁴.

The stability of the lasing solution (3) against space-dependent perturbations has been also investigated^{1,3}. A linear stability analysis predicts that a pattern forming instability of the homogeneous state occurs for pump values below a critical value or, alternatively, above a critical detuning value. The analytical expressions are rather involved, but the instability threshold can be found in particular cases numerically. In Fig. 1 we represent the domain of existence of the different solutions in the plane $\langle \Delta_1, E \rangle$. The homogeneous solution exists above line (a), being stable to the left of the dashed line (c) and unstable versus the roll pattern to the right of line (c). The roll pattern appearing in this region has a dc component, at difference with the roll pattern appearing for negative detuning, which has no dc component and thus its visibility equals unity. In the region marked as BS, between lines (a) and (b), the trivial and homogeneous solutions coexist but as the latter is modulationally unstable, in this region bright cavity solitons are formed^{1,26}.

3. Nonequilibrium Ising–Bloch transition

In this section we report the results of our numerical study of the DW dynamics. We integrated numerically Eqs. (1) and (2) making use of a split-step algorithm with periodic boundary conditions. Spatial grids from 1024 to 8192 points were used in order to check convergence. Results reported here were obtained with an integrating window length $L = 316$ (other values were also used) and the temporal step was lowered up to $\delta t = 10^{-2}$ in order to yield δt –independent results. We considered two cases for the pump amplitude profile E corresponding to (i) an infinitely extended plane-wave field and (ii) a flat but spatially limited field, flat in order to avoid any gradient effect on the DW dynamics. For this last case we chose

$$E = E_0 \exp \left[- (x/\Delta x)^8 \right], \quad (4)$$

with $\Delta x = 0.45L$, which is top-hat like: it is flat around $x = 0$ and null close to the border of the integration region ($x = \pm L/2$). This supergaussian profile is used with the only purpose of simulating a flat and finite pump and that is not essential for the results here reported. In fact very similar results, differing mainly on minor quantitative details, are found in the two studied cases, thus demonstrating the robustness of the reported behaviour.

We first report the results obtained for a top-hat pump. A wall connecting the two homogeneous, oppositely phased states was excited by using an appropriate initial condition. The two kinds of walls, Ising and Bloch, were found at different parameter values. Whilst the intensity trace $|A_1(x)|^2$ of the walls formed in the subharmonic field does not allow to distinguish clearly between Ising and Bloch walls -due to the very small value of the intensity at the core of the wall- the different nature of the walls can however be clearly appreciated in a parametric representation $\langle \text{Re } A_1, \text{Im } A_1 \rangle$ of these interfaces. In Fig. 2 the parametric representations of both an Ising wall, Fig. 2(a), obtained for $E_0 = 3$ and $\Delta_1 = 1.2$, and a Bloch wall, Fig. 2(b), obtained for $E_0 = 3$ and $\Delta_1 = 1.5$, are shown. The NIB transition, numerically computed from Eqs.(1) and (2), is plotted in Fig. 1, line (d).

The NIB transition can be clearly identified as a bifurcation of a chirality parameter defined as¹⁸

$$\chi = \text{Im} [A_1^*(x_0) \partial_x A_1(x_0)], \quad (5)$$

where x_0 is the position of the wall core, i.e. where $|A_1|$ is closest to zero. Notice that if we use a polar decomposition of $A_1(x)$ as $A_1(x) = |A_1(x)| \exp[i\phi_1(x)]$, then $\chi = |A_1(x_0)|^2 \partial_x \phi_1(x_0)$. Thus this quantity is sensitive to both the sense and magnitude of the rotation of the phase angle at the wall, $\partial_x \phi_1(x_0)$, and to the intensity at the wall core, $|A_1(x_0)|^2$. Consequently $\chi = 0$ for Ising walls and $\chi \neq 0$ for Bloch walls, and the NIB can be understood as a pitchfork bifurcation of the chirality parameter.

As Eqs. (1) and (2) are invariant under spatial translations ($x \rightarrow x + x'$) and spatial reflections ($x \rightarrow -x$), if a Bloch wall $A_1^{(1)} = A_B(x - x_0, t)$ exists with chirality χ_1 another Bloch wall $A_1^{(2)} = A_B(x_0 - x, t)$ also exists and has chirality $\chi_2 = -\chi_1$. This is important,

as a generic property of domain walls in nongradient systems (at least for domain walls of the tanh type) is that they move with a velocity which is proportional to their chirality¹⁴, so that Bloch walls with opposite chiralities move in opposite directions, and Ising walls ($\chi = 0$) are at rest.

In Fig. 3 the signal field intensity $|A_1(x)|^2$ is shown for the same set of parameters as in Fig. 2(a), and the Ising wall is clearly appreciated in the center of the illuminated region, where it remains at rest indefinitely. In Fig. 4(a) a similar representation for the same parameters as in Fig.2 (b), that is, for a Bloch wall, is shown. In this case the position of the wall varies with time as can be seen in Fig. 4(b), which displays the time evolution of the wall position: contrarily to the Ising wall, the Bloch wall drifts at a velocity v (that depends on the parameter values) until it reaches the boundary of the pumped area, where it remains locked.

Let us notice that, in the wall neighbourhood, the intensity profile of the signal field shows spatial oscillations that decay exponentially to the homogeneous state given by (3), see Figs. 3 and 4. These spatial modulations appear in the parametric representation as a spiralling of the heteroclinic trajectory around the stable fixed points representing the homogeneous stable solutions, see Fig. 2. These modulations have a characteristic wavenumber that can be predicted by a spatial stability analysis²⁵, and are typical of diffraction-supported fronts. These modulations play an important role in the stabilization of the walls, and allow for the existence of bounded states²⁵. The number of orbits in the parametric representation increases when approaching the pattern forming instability boundary, line (c) in Fig. 1.

4. Nonlinear dynamics of the Bloch wall

We consider next the dynamical properties of Bloch walls. First we consider the case of the top-hat pump profile of Eq.(4) and then we consider the case of plane-wave pumping. In both cases, a typical route is reported, as obtained for $E = 3$, and the signal detuning Δ_1 is left as the control parameter.

A. Pump field with finite transverse extension

The Ising wall represented in Fig. 3 (also in Fig. 2 (a)), corresponding to $\Delta_1 = 1.2$, suffers instabilities at its core by increasing Δ_1 . For the selected pump value, the NIB transition is found at $\Delta_1 = 1.362$. At this point the value of the intensity at the dip becomes different from zero, although it has an extremely small value, and the wall starts to move with a constant drift, as shown in Fig. 4 for $\Delta_1 = 1.5$. We note that the drift velocity of the wall is not exactly constant as it slightly oscillates with a very low frequency. We shall return to this point in the next section.

For detuning values larger than $\Delta_1 = 1.73$ the homogeneous solution (3) becomes modulationally unstable, see Fig. 1, and each of the two domains connected by the wall develop extended spatial oscillations. Bloch walls still exist in this parameter region but now they connect two patterned states instead of two homogeneous solutions⁴. This type of domain wall was already found in the PDNLS¹⁸. An example of the intensity profile of a wall affected by the modulational instability is shown in Fig. 5, corresponding to $\Delta_1 = 2.01$. For this value of the detuning, after a transient the wall moves at nearly constant velocity until it reaches the border of the illuminated region, where it remains locked, see Fig. 5(b), similarly to the case of Fig. 4(b). Notice however that now the wall is bounced from the border of the illuminated region before it locks to it. Further increasing the detuning, the Bloch wall keeps existing but exhibits an erratic motion until finally it is also locked to the boundary. This "chaotic" motion of the Bloch walls is observed for $\Delta_1 > 2.03$.

We see that with a pump of finite extension, the dynamics of the domain walls is always transient as Bloch walls get eventually locked to the boundary of the illuminated region. Then in order to quantitatively analyze the temporal dynamics of Bloch walls, it is necessary to consider an infinitely extended plane-wave pump in order to avoid the influence of boundary effects. This is done in the next subsection.

B. Infinitely extended pump field

For periodic boundary conditions and uniform pump, an even number of DWs had to be excited. In our simulations, two DWs were initially created. Consequently care had to be taken that the two DWs did not interact as the dynamics of a single DW was to be studied. This was done by checking that the two domain walls were far apart each other and that they did not approach significantly during the numerical run. We analyzed the temporal series of both the chirality and velocity of DWs. In Fig. 6 the dependence of both quantities on the detuning Δ_1 are shown for a pump value $E = 3$. Next we analyze this bifurcation diagram in detail.

The NIB occurs at $\Delta_1 = 1.362$, as in the case of spatially limited pump, and at this point both the chirality and velocity of the wall become non-null through a pitchfork bifurcation. Nevertheless, for detunings slightly below this value there appears some subtle dynamics, as anticipated. For a detuning of $\Delta = 1.361$ we have observed that the position of the DW oscillates in time, with null mean displacement and a very small amplitude in the oscillations (of the order of a fraction of a pixel - the determination of the intensity minimum was done through a three-point parabolic fit). In Fig.7 (a) the power spectrum of the chirality time series corresponding to this case is shown. The frequency of the oscillation is so small ($f = 1.793 \cdot 10^{-4}$) that runs with a duration $\Delta t = 2^{18}$ (more than 26 milion time steps) had to be considered in order to have 47 oscillations. Given the tiny value of the fundamental frequency, power spectra were obtained after sampling every time unit. In Fig. 7(b) the power spectrum corresponding to a detuning $\Delta_1 = 1.365$, that is beyond the NIB transition, is shown. The fundamental frequency in the spectrum is larger than that in Fig. 7(a) and, remarkably, the dynamics is richer as higher order harmonics appear. In the range of detunings $1.362 < \Delta_1 < 1.85$, the movement of the wall is practically steady but for these very low frequency, smallest amplitude, oscillations; that is, for constant detuning the velocity is very nearly constant, its value increasing with the detuning as can be seen in Fig. 6. Unfortunately, as the NIB transition is crossed, it is no more possible to track the

low frequency dynamics as new oscillatory bifurcations involving much higher frequencies develop. Thus, up to $\Delta_1 = 1.85$ the velocity of the Bloch wall is not constant but the frequency of the oscillation, as well as its amplitude, is so small that one can consider it as practically constant. In the following we neglect this low frequency dynamics.

At $\Delta_1 = 1.85$ there is a clear Hopf bifurcation at which the velocity is no more constant but begins to oscillate in time (in Fig. 6 we plot both the maximum and minimum values of the velocity and chirality in this oscillatory regime). In Fig. 8(a) the spectrum corresponding to that clear periodic motion is shown. Let us remark that the frequency of these oscillations is larger, by a factor greater than 350, than the low frequency oscillations above commented.

It is most interesting to notice that this Hopf bifurcation occurs at exactly the same detuning value at which the homogeneous solution of the system becomes modulationally unstable, line (c) in Fig.1. This does not seem to be accidental or specific of this system as we have observed the same phenomenon in the PDNLS equation^{18,28}. Then it seems that the appearance of a Hopf bifurcation in the movement of the Bloch wall is forced by the modulational instability that the homogeneous solution undergoes. Up to some extent this fact can be understood intuitively. The appearance of a pattern on the background where the domain wall exists necessarily influences the movement of the domain wall as the displacement of the wall forces local changes in the spatial frequency of the pattern. On their turn, these local readjustments in the pattern shape modify the velocity of the Bloch wall. This is consistent with the fact that the oscillations developed by the wall velocity increase their amplitude as the detuning is increased, as it occurs with the modulation of the roll pattern on which the wall is "written".

Further increasing the detuning leads to the appearance of new frequencies in the spectrum. At $\Delta_1 = 1.93$, a new and incommensurate frequency appears, see Fig. 8(b), reflecting the fact that the movement of the wall is now quasiperiodic. At $\Delta_1 = 1.95$, there still appears a third new incommensurate frequency, and then the movement of the wall corresponds to a 3-torus dynamics, Fig. 8(c). This quasiperiodic dynamics remains up to $\Delta_1 = 2.014$. In Fig. 9 we represent a projection of the attractor on the $\langle v, \chi \rangle$ plane for a periodic and a

quasiperiodic behaviour, see caption. Notice in Fig. 6(a) that at $\Delta_1 \approx 1.96$, the minimum value of the chirality becomes negative, although the velocity remains positive along all the depicted lines (see also Fig. 9(b)). This means that, under oscillatory dynamics, there is no more a direct relation between the sign and magnitude of the chirality and those of the velocity.

We find it important to emphasize that the observed dynamics is due to the existence of a DW: we have checked that the roll pattern existing for $\Delta_1 > 1.73$ is always steady for $E = 3$. Then, the secondary bifurcations affecting the Bloch wall movement are not induced by any temporal dynamics of the pattern, but have to be attributed to the interplay between the change in the wall velocity with detuning, on the one side, and the changes in the spatial frequency and modulation of the roll pattern, on the other side.

For detuning values within the range $2.014 < \Delta_1 < 2.017$ (within the shaded area depicted in Fig. 6) the dynamic behaviour of the wall cannot be tracked as the two excited walls always coalesce into a single structure (a cavity soliton). Although we tried to avoid this fact by changing the initial conditions (more specifically, the initial chirality value of the two walls) we have not been able of isolating the dynamics of a single structure in this smallest domain of detunings.

Further, at $\Delta_1 = 2.017$, there appears a new qualitative change in the dynamics of the Bloch wall: the time evolution of the chirality (or the velocity) is again periodic but now the dynamics correspond to an attractor different from the one shown in Fig. 9, as can be seen in Fig. 10(a). This new attractor is two sided, that is, the orbit on the $\langle v, \chi \rangle$ plane surrounds alternatively the two unstable symmetric fixed points differing in the sign of the chirality and the velocity. As in the previous case, this periodic attractor transforms into a chaotic one, Fig. 10(b), after a series of bifurcations involving tori, see Fig. 11. However, in this case the route to chaos is quite unusual: By increasing the detuning, this motion remains periodic until $\Delta_1 = 2.0250$, then at $\Delta_1 = 2.0251$ the motion becomes quasiperiodic and at $\Delta_1 = 2.0252$ an intermittent route to chaos (built on the torus) is initiated. Close to this border laminar phases are very long and become shorter as we move from the bifurcation,

as usual. An example of this intermittent behaviour is shown in Fig. 12 where a series of chirality extrema is depicted. We have not tried to characterize this highly complicated behaviour and just note that the same type of intermittencies were found by some of us in laser models^{29,30}. Further increasing detuning laminar phases become progressively shorter until eventually they disappear (at some detuning value between 2.035 and 2.039) the wall motion becoming chaotic. For still larger values of the detuning, the dynamics of the wall remains chaotic until line (b) in Fig.1 is crossed as at this point the pattern is no more stable and bright (sech type) solitons appear after a transient.

5. Conclusions

We have presented numerical evidence of the existence of a nonequilibrium Ising-Bloch transition in a type-I DOPO model with one transverse dimension. Bloch walls have been found in two different forms, either connecting homogeneous states, which are the usual ones, or connecting modulated states, a kind of domain wall already found in the propagation model for DOPO⁴, and in the parametrically driven, damped nonlinear Schrödinger equation¹⁸.

Bloch walls move and their movement undergoes complicated secondary bifurcations eventually leading to chaotic motion involving quasiperiodicity. Two routes to chaos have been described: A usual quasiperiodic (Ruelle-Takens) scenario and an unusual quasiperiodic intermittency. We have seen that the nonlinear dynamics of the wall movement is related to the appearance of a modulational instability on the pattern on which the domain wall is written. Let us remark that although the NIB transition in DOPO has been reported for the particular case $\Delta_0 = 2\Delta_1$, we have observed similar phenomena for different sets of detuning values. In fact, for the case of large pump detuning (and signal detuning of order one), the DOPO equations can be approximated by the PDNLS equation¹, where the NIB transition as well as the nonlinear dynamics of the Bloch wall have been previously reported by some of us^{18,28}.

We would like to finish with a brief mention to the case of two transverse spatial di-

mensions. In 2D the situation is by far much more complicated than the 1D case we have analyzed here, as in 2D the dynamics of DWs is affected not only by the NIB but also by curvature effects^{6,4}. Moreover, boundary effects become determinant in two dimensions as domain walls tend to be perpendicular to the boundary of the illuminated region. Then the analysis of the NIB in a two dimensional optical system still remains to be characterized.

We thank Javier Redondo (Departament de Física Aplicada, Universitat Politècnica de València) for useful discussions about the processing of the numerical data. This work has been supported by the Spanish Ministerio de Ciencia y Tecnología and the European funds FEDER under projects BFM2002-04369-C04-01 and BFM2002-04369-C04-04.

REFERENCES

1. S. Longhi, Phys. Scr. **56**, 611 (1997).
2. S. Trillo, M. Haelterman and A. Sheppard, Opt. Lett. **22**, 970 (1997).
3. K. Staliunas and V.J. Sánchez-Morcillo, Phys. Rev. A **57**,1454 (1998).
4. M. Le Berre, D. Leduc, E. Ressayre, and A. Tallet, J. Opt. B: Quantum Semiclass. Opt. **1**, 153 (1999).
5. I. Rabiosi, A.J. Scroggie, and G.-L. Oppo, Phys. Rev. Lett. **89**, 254102 (2002).
6. G.Izús, M. San Miguel and M. Santagiustina, Opt. Lett. **25**, 1454 (2000).
7. V.J. Sánchez-Morcillo, I. Pérez-Arjona, F. Silva, G.J. de Valcárcel, and E. Roldán, Opt. Lett. **25**, 957 (2000).
8. D. Michaelis, U. Peschel, F. Lederer, D.V. Skryabin and W.J. Firth, Phys. Rev. E **63**, 066602 (2001).
9. V.B. Taranenko, K. Staliunas and C.O. Weiss, Phys. Rev. Lett. **81**, 2236 (1998).
10. Ye. Larionova, U. Peschel, A. Esteban-Martín, J. García-Monreal, and C.O. Weiss, submitted (2003).
11. M. Tlidi, P. Mandel and R. Lefever, Phys. Rev. Lett. **81**, 979 (1998).
12. E. Grosse Westhoff. V. Kneisel, Yu A. Logvin, T. Ackemann, and W. Lange, J. Opt. B: Quantum Semiclass. Opt. **2**, 386 (2000).
13. L.N. Bulaevskii and V.L. Ginzburg, Sov. Phys. JETP **18**, 530 (1964); J. Lajzerowicz and J. J. Niez, J. Phys. (Paris) Lett. **40**, L165 (1979).
14. P.Couillet, J. Lega, B. Houchmanzadeh and J. Lajzerowicz, Phys. Rev. Lett. **65**, 1352 (1990).
15. T. Frisch, S. Rica, P.Couillet amd J. M. Gilli, Phys. Rev. Lett. **72**, 1471 (1994).

16. A. Hagberg and E. Meron, Phys. Rev. E **48**, 705 (1993).
17. D.V. Skryabin, A. Yulin, D. Michaelis, W.J. Firth, G.-L. Oppo, U. Peschel, and F. Lederer, Phys. Rev. E **64**, 056618 (2001).
18. G.J. de Valcárcel, I. Pérez–Arjona, and E. Roldán, Phys. Rev. Lett. **89**, 164101 (2002).
19. J. W. Miles, J. Fluid Mech. **148**, 451 (1984).
20. C. Elphick and E. Meron, Phys. Rev. A **40**, 3226 (1989).
21. A. Mecozzi, W.L. Kath, P. Kumar, C.G. Goedde, Opt. Lett. **19**, 2050 (1994).
22. G. L. Oppo, M. Bambrilla and L. A. Lugiato, Phys. Rev. A **49**, 2028 (1994).
23. L.A. Lugiato, C.Oldano, C. Fabre, E. Giacobino and R.J. Horowicz, Nuovo Cimento D **10**, 959 (1988).
24. G.J. de Valcárcel, K. Staliunas, E. Roldán, and V.J. Sánchez-Morcillo, Phys. Rev. A **54**, 1609 (1996).
25. V.J. Sánchez-Morcillo and K. Staliunas, Phys. Rev. E **61**, 7076 (2000).
26. K. Staliunas and V.J. Sánchez-Morcillo, Opt. Commun. **139**, 306 (1997).
27. J.-P. Eckmann and I. Procaccia, Phys. Rev. Lett. **66**, 891 (1991).
28. I. Pérez–Arjona, *Transicions Ising–Bloch en l’Equació Nolineal d’Schrödinger amb Decaïment i Forçament Paramètric*, (Universitat de València, 2001), unpublished.
29. G.J. de Valcárcel, E. Roldán, V. Espinosa and R. Vilaseca, Phys. Lett. A **206**, 359 (1995); **209**, 388(E) (1995)
30. J. Redondo, G.J. de Valcárcel, and E. Roldán, Phys. Rev. E **56**, 6589 (1997).

Figure captions

Fig. 1. Bifurcation diagram in the parameter space pump amplitude (E) vs. signal detuning (Δ_1). The different lines denote: (a) the location of the turning point of the homogeneous, "lasing" solution; in (b) the trivial solution loses its stability; in (c) the homogeneous solution (that is stable to the left of this line and unstable to the right) suffers a modulational instability that gives rise to the appearance of patterns; finally, line (d) denotes the location of the Ising–Bloch transition. The region denoted by BS corresponds to the bistability domain where bright solitons can be excited.

Fig. 2. Parametric representation of an Ising (a) and a Bloch (b) wall, computed numerically from Eqs. (1) with $E = 3$ and (a) $\Delta_1 = 1.2$, and (b) $\Delta_1 = 1.5$.

Fig. 3. Intensity profile of the signal field, $|A_1|^2$, as a function of the normalized position x/L for $E = 3$ and $\Delta_1 = 1.2$. An Ising wall appears at the center.

Fig. 4. (a) As in Fig.3 but for $E = 3$ and $\Delta_1 = 1.5$ showing a Bloch wall. (b) Time evolution of the pattern. The pattern in (a) corresponds to $t = 400$ in the time evolution shown in (b).

Fig. 5. As in Fig.4 but for $E = 3$ and $\Delta_1 = 2$.

Fig. 6. Bifurcation diagram for the Chirality (a) and velocity (b) of the wall as a function of detuning for $E = 3$. I denotes the region of existence of Ising walls and B the region of existence of Bloch walls with constant velocity. In P the motion of Bloch walls is periodic (quasiperiodic in T and T^2 , and chaotic in C) and the maximum and minimum value of the chirality and velocity are represented. The inset diagram show the dynamics in the grey region, where Int correspond with the intermittent route to chaos and the symbol (?) marks the detuning where the dynamics of a single wall cannot be tracked (see text).

Fig. 7. Chirality spectrum for the time series corresponding to $E = 3$, $\Delta_1 = 1.361$ (a) and $\Delta_1 = 1.365$ (b).

Fig. 8. Chirality spectrum for the time series corresponding to $E = 3$, $\Delta_1 = 1.86$ (a), $\Delta_1 = 1.93$ (b) and $\Delta_1 = 1.99$ (c); that correspond to regions P , T , and T^2 in the diagram

in Fig.6.

Fig. 9. Attractor projection on the $\langle v, \chi \rangle$ plane for (a) $E = 3$ and $\Delta_1 = 1.86$ (periodic attractor) and $E = 3$ and $\Delta_1 = 1.99$ (quasiperiodic attractor).

Fig. 10. Attractor projection on the $\langle v, \chi \rangle$ plane for (a) $E = 3$ and $\Delta_1 = 2.02$ (periodic two-sided attractor) and (b) $E = 3$ and $\Delta_1 = 2.04$ (chaotic attractor) corresponding to regions P and C , in the inset in Fig.6.

Fig. 11. Chirality spectrum for the time series corresponding to $E = 3$ and $\Delta_1 = 2.02$ (a), $\Delta_1 = 2.0251$ (b) and $\Delta_1 = 2.04$ (c); corresponding to regions P , T , and C in the inset diagram in Fig. 6.

Fig. 12. Series of chirality extrema for $E = 3$ and $\Delta_1 = 2.0260$, corresponding to the intermittent route to chaos in the inset in Fig.6.

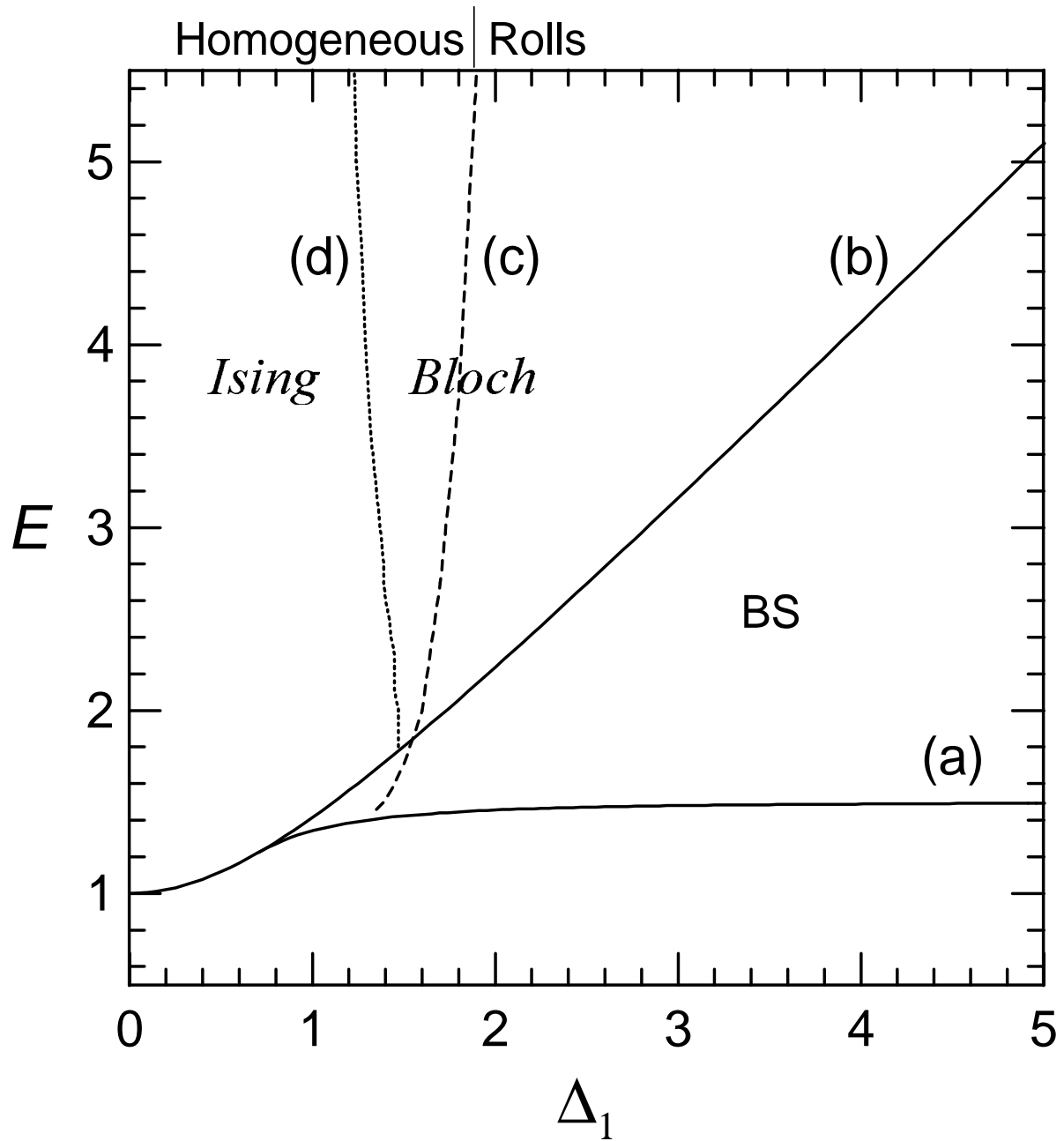


Figure 1.-
Nonequilibrium Ising-Bloch transition ...

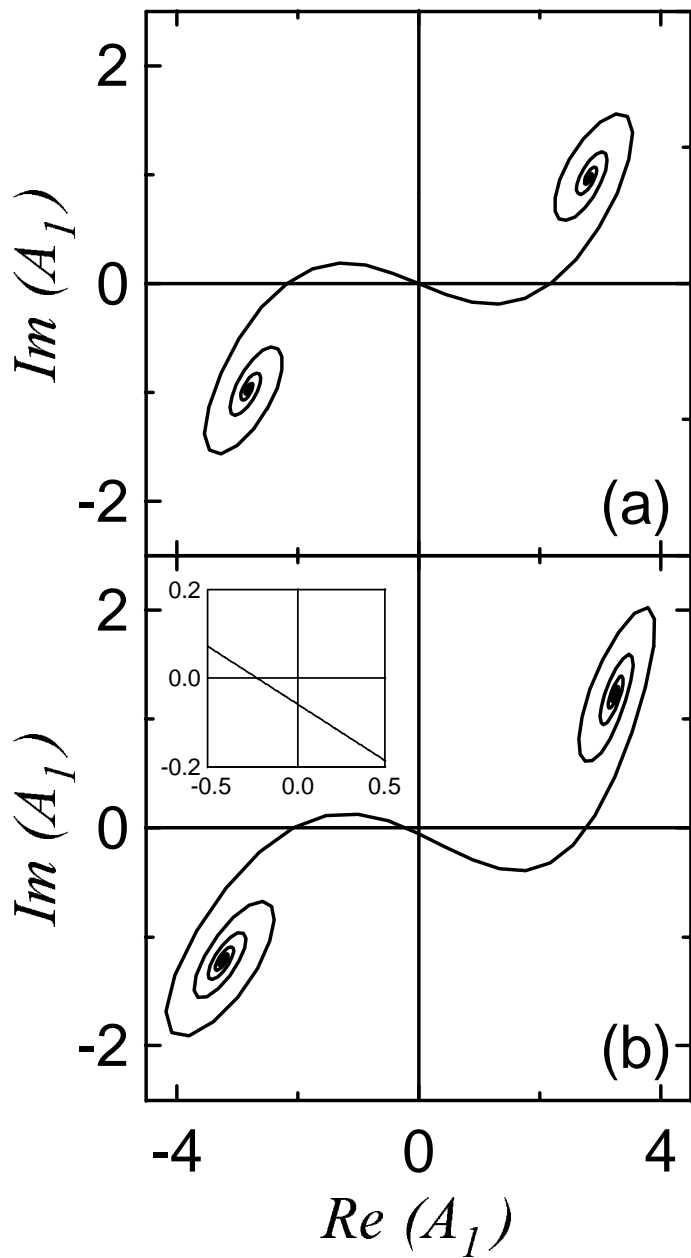


Figure 2.-
Nonequilibrium Ising-Bloch transition ...

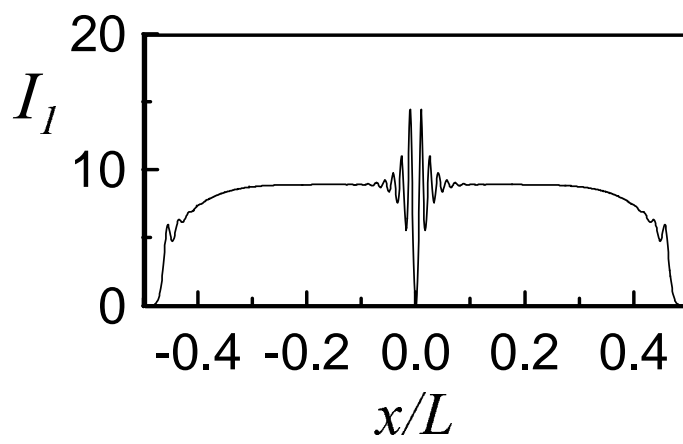


Figure 3.-
Nonequilibrium Ising-Bloch transition ...

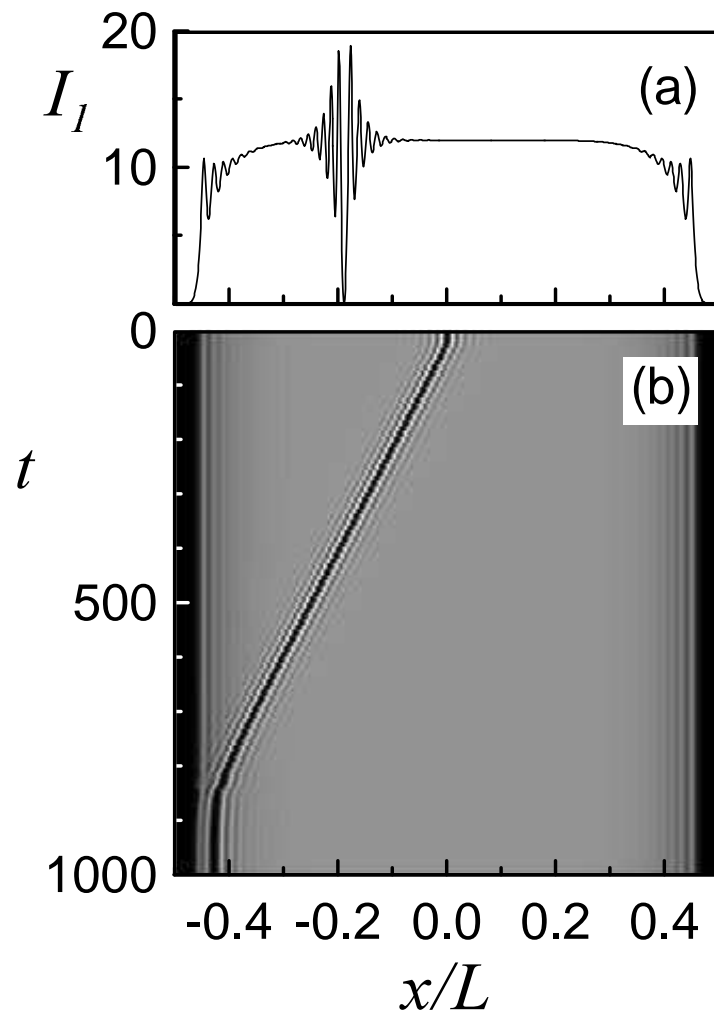


Figure 4.-
Nonequilibrium Ising-Bloch transition ...

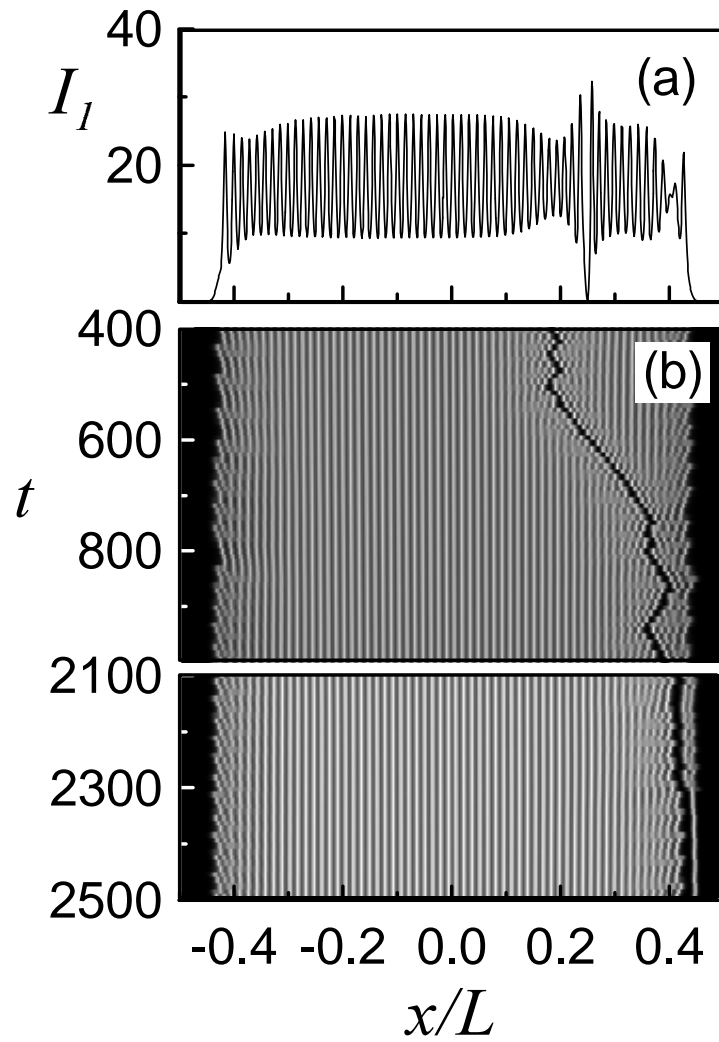


Figure 5.-
Nonequilibrium Ising-Bloch transition ...

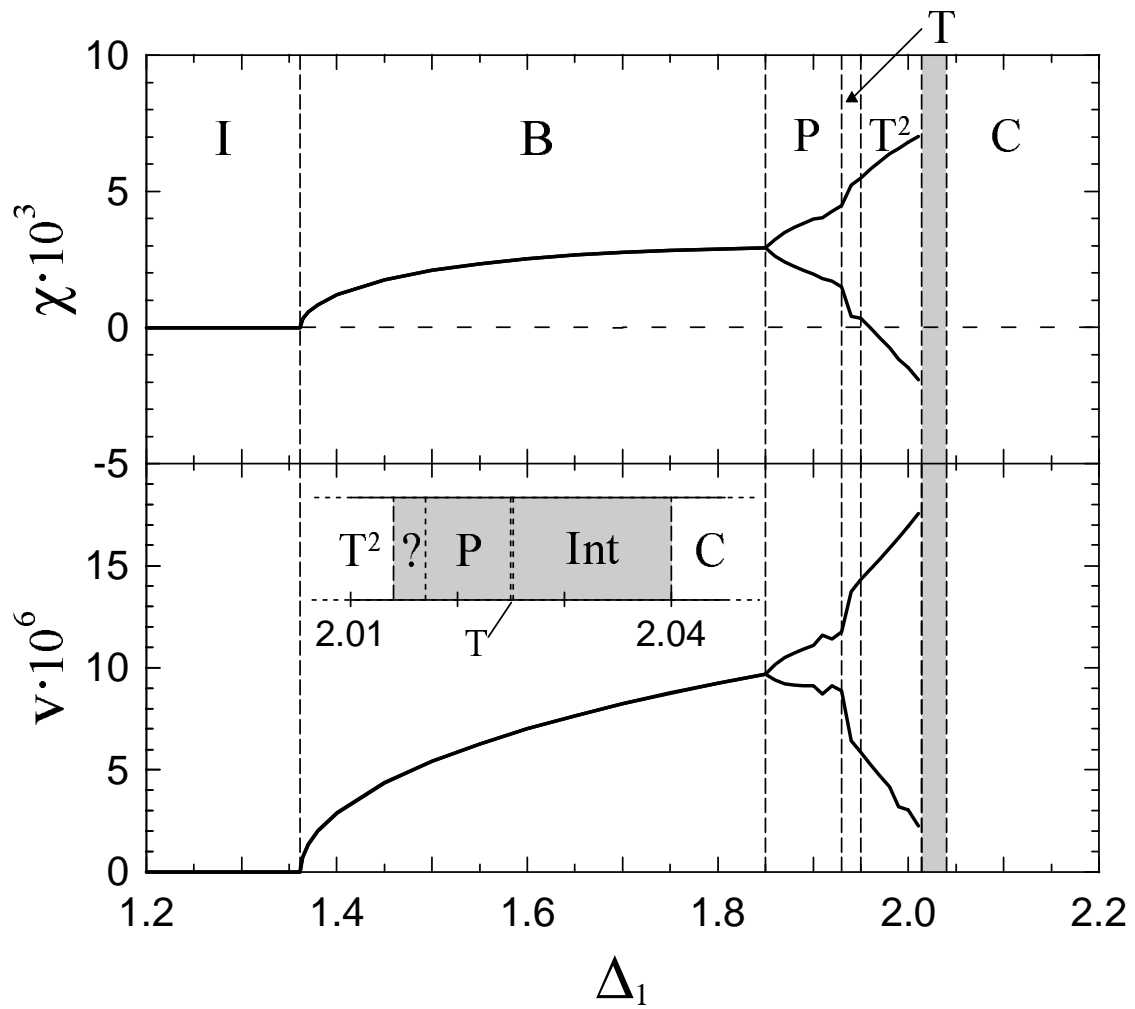


Figure 6.-
Nonequilibrium Ising-Bloch transition ...

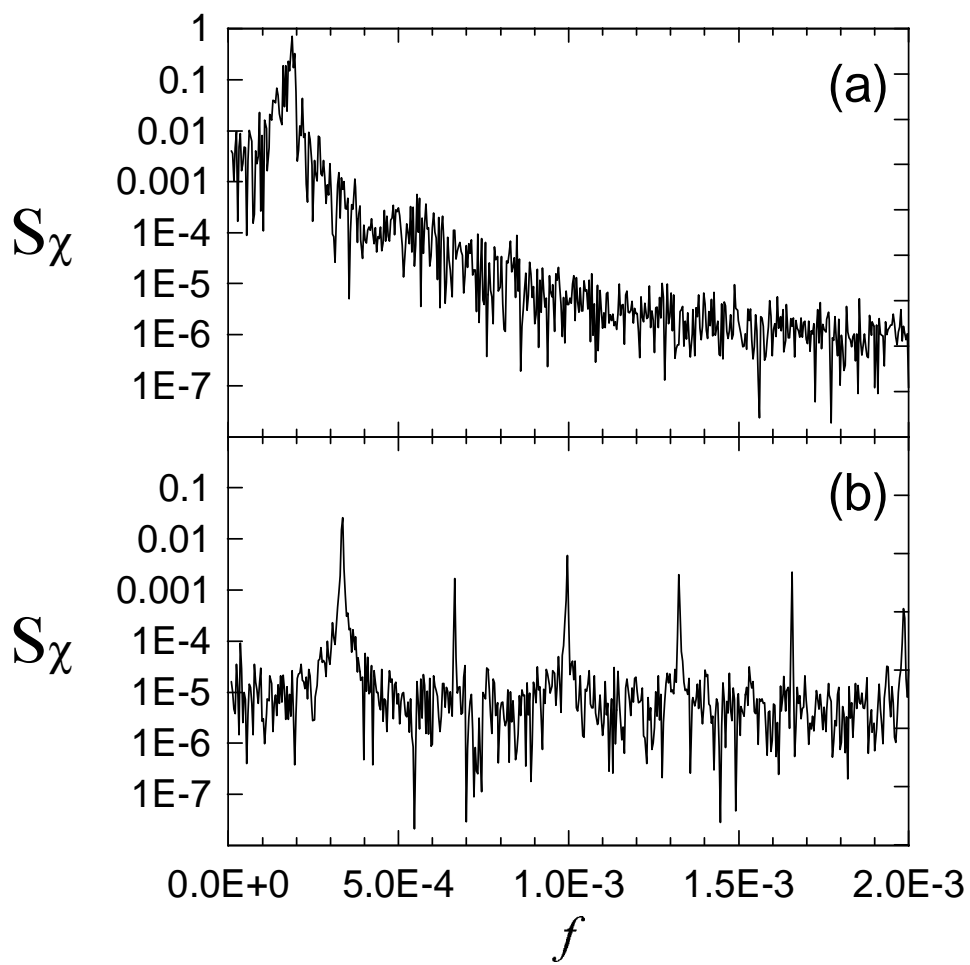


Figure 7.-
Nonequilibrium Ising-Bloch transition ...

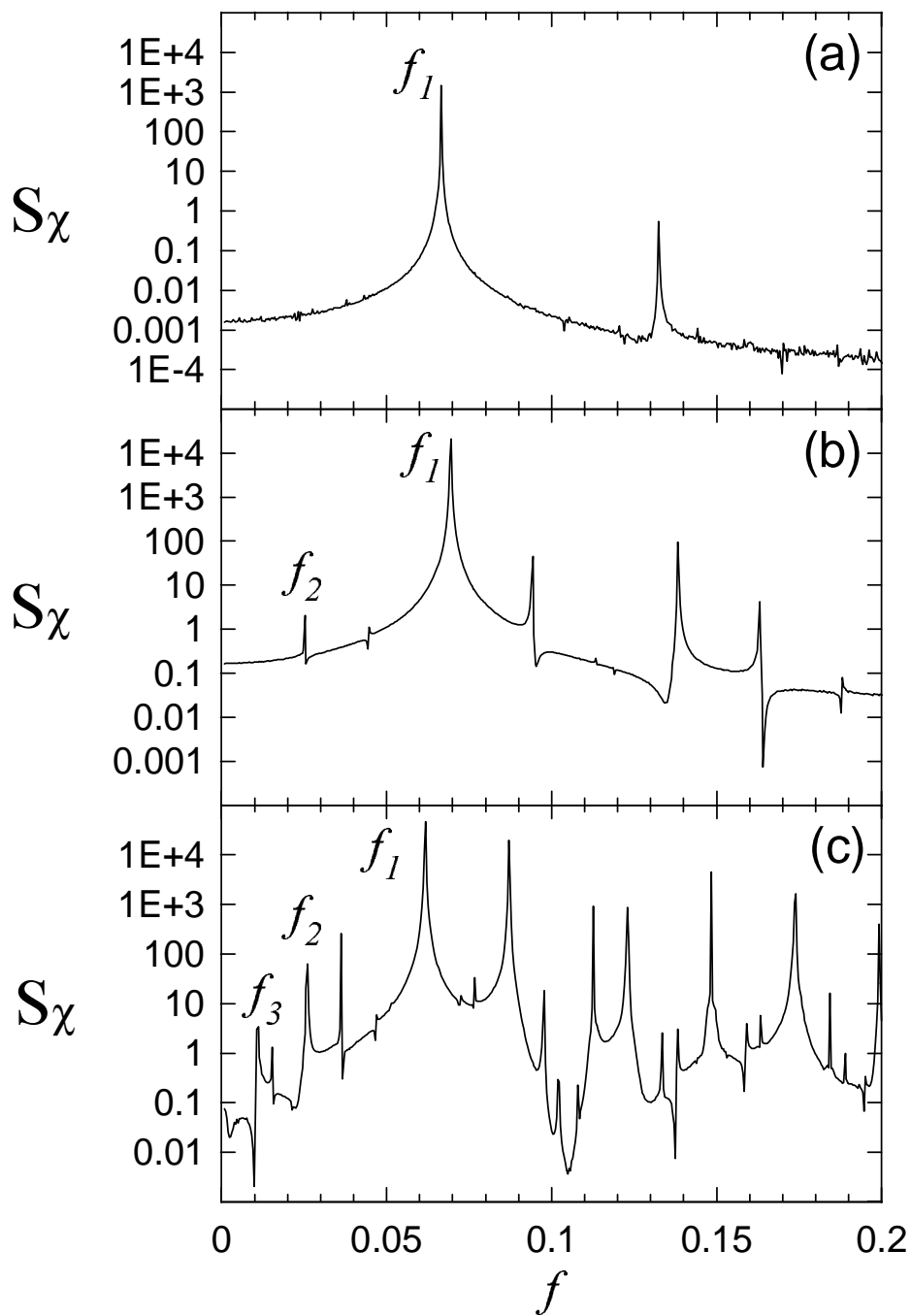


Figure 8.-
Nonequilibrium Ising-Bloch transition ...

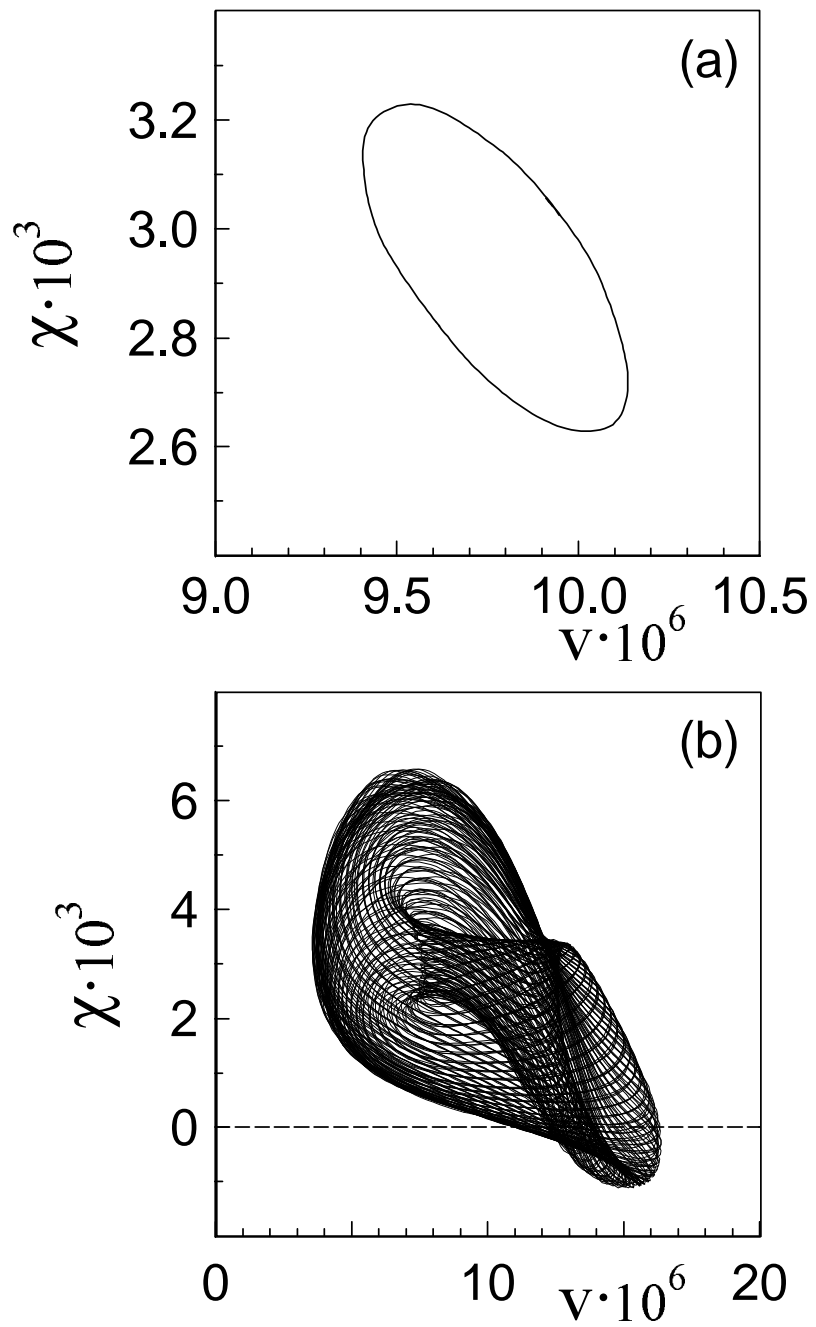


Figure 9.-
Nonequilibrium Ising-Bloch transition ...

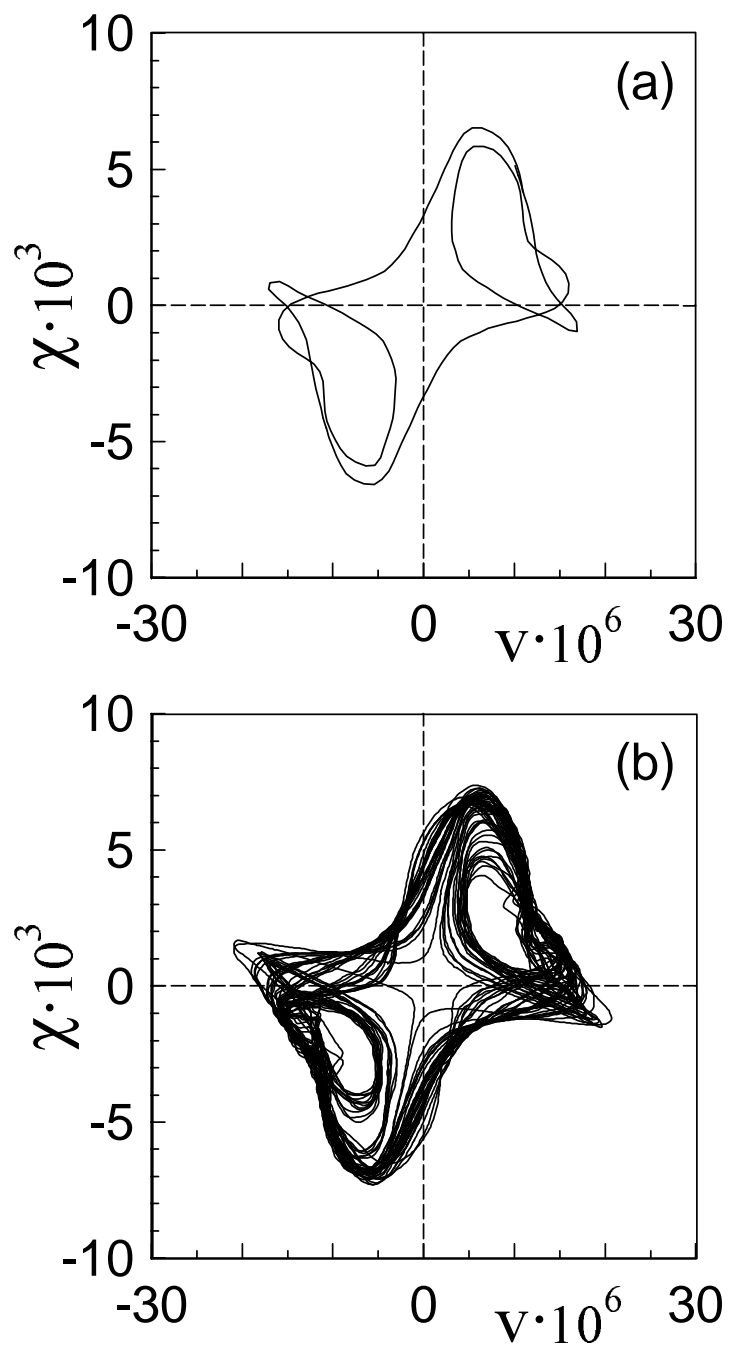


Figure 10.-
Nonequilibrium Ising-Bloch transition ...

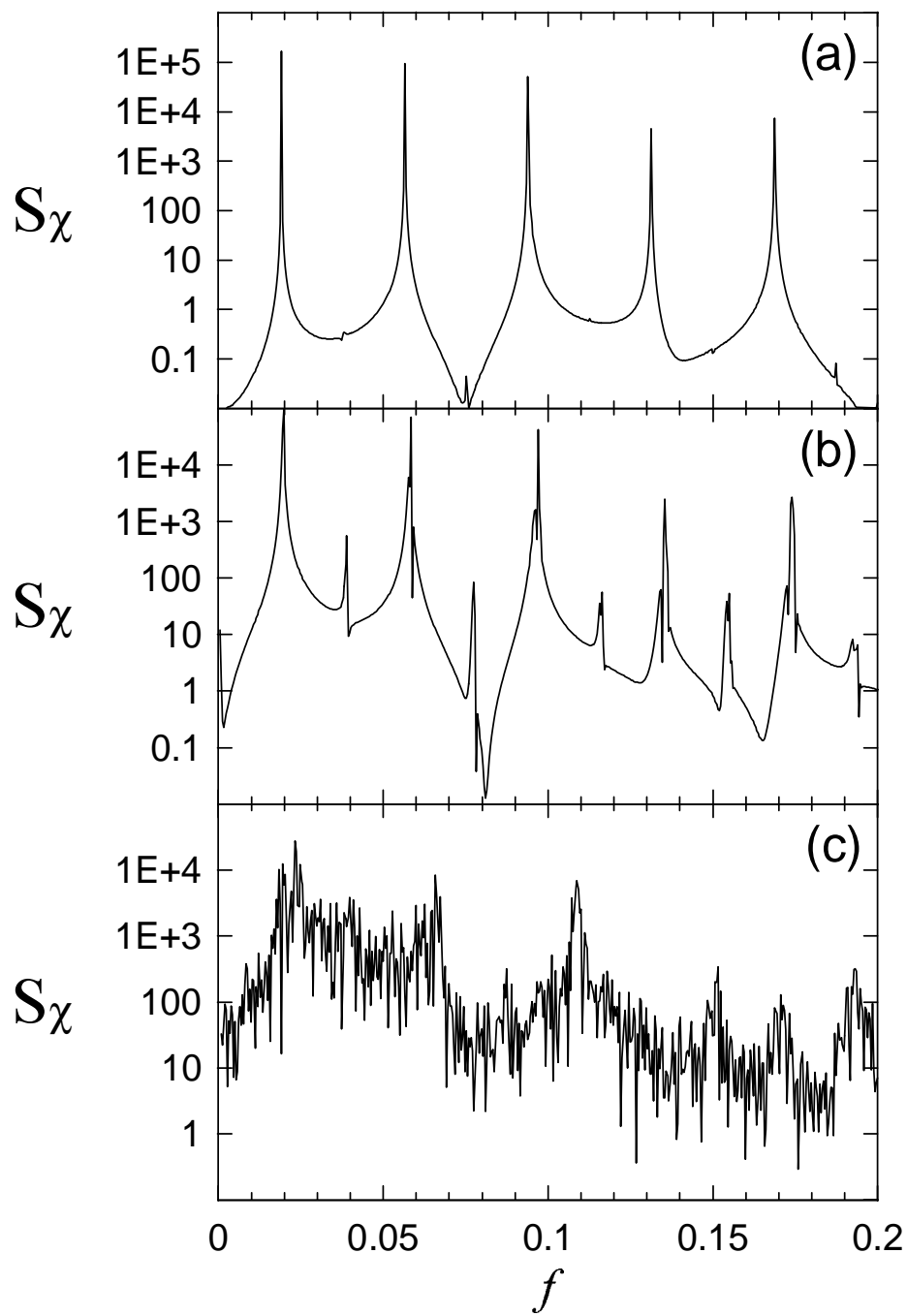


Figure 11.-
Nonequilibrium Ising-Bloch transition ...

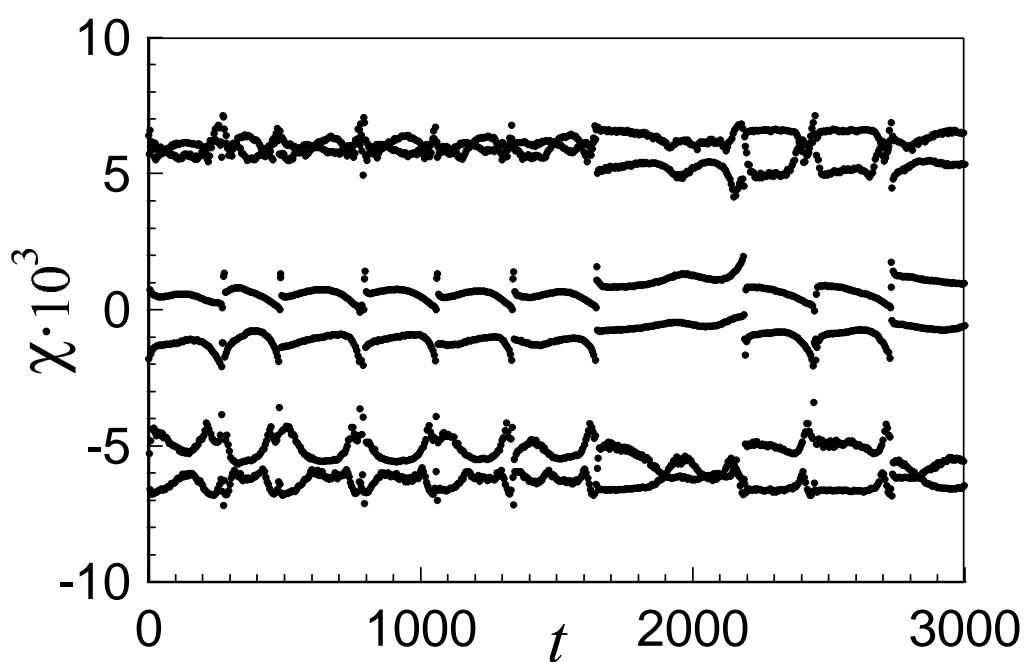


Figure 12.-
Nonequilibrium Ising-Bloch transition ...